NASA

Technical Memorandum 83903

(NASA-TM-83903) N82-21828
COAST-OCEAN-ATMOSPHERE-OCEAN MESOSCALE
INTERACTION (NASA) 32 p HC A03/MF A01
CSCL 04B Unclas
G3/47 18791

COAST-OCEAN-ATMOSPHERE-OCEAN MESOSCALE INTERACTION

David Atlas and Shu-Hsien Chou
Goddard Laboratory for Atmospheric Sciences
NASA/Goddard Space Flight Center

FEBRUARY 1982

National Aeronautics and
Space Administration

Goddard Space Flight Center
Greenbelt, Maryland 20771

COAST-OCEAN-ATMOSPHERE-OCEAN MESOSCALE INTERACTION

ABSTRACT

In the case of cold air outbreaks, the combination of the coastal shape and the sea surface temperature (SST) pattern has been shown to have a profound effect in establishing a low level mesoscale atmospheric circulation as a result of differential heating due to both variations in over-water path length and the SST. A convergence (or divergence) line then forms along a line exactly downwind of the major bend in the coastline. All this is consistent with the structure of the cloud patterns seen in a high resolution Landsat picture of the cloud streets and the major features are simulated well with a boundary layer model. The dominant convergence line is marked by notably larger clouds. To its east the convective roll clouds grow downstream in accord with the deepening of the boundary layer. To its west (i.e., coastal side) where the induced pressure field forces a strong westerly component in the boundary layer, the wind shear across the inversion gives rise to Kelvin-Helmholtz waves and billow clouds whose orientation is perpendicular to the shear vector and to the major convergence line. It is also suggested that the induced mesoscale circulation will feedback on the ocean by intensifying the wind-generated ocean wave growth and altering their orientation. We postulate that coastal cyclogenesis is due in large part not only to the fluxes of heat and moisture from the ocean, as has been proposed by many authors, but particularly to the differential heating and moistening of the boundary layer air when the air trajectories pass over a well defined pattern of SST. With east to northeasterly winds, Cape Hatteras lies downstream of the Gulf Stream core, thereby providing a possible explanation for the notably high frequency of cyclogenesis in that region.

COAST-OCEAN-ATMOSPHERE-OCEAN MESOSCALE INTERACTION

1. Introduction

In the accompanying article in this issue Chou and Atlas (1982), hereafter referred to as I, discuss a satellite-based method of deducing the sensible and latent heating of the atmosphere by the fluxes from the ocean during cold air outbreaks. In that study we used imagery from both TIROS-N and GOES to observe the so-called "cloud free path" or CFP, the structure and orientation of the cloud streets, and the sea surface temperature (SST) between shore and the cloud edge. In order to deduce the rate of deepening of the convective boundary layer downstream along the flow, we attempted to use the IR cloud top temperatures observed by the TIROS-N Advanced Very High Resolution Radiometer (AVHRR). We found this to be impossible because most of the clouds near the line of initial cloud formation did not fill the 1 x 1 km field of view of the radiometer. However, we were fortunate to find that Landsat-3 with its 80 m resolution passed over the area of interest off the coast of New Jersey on the day of our study. The accompanying picture, Fig. 1, having dimensions of 180 x 340 km is a composite of two Landsat frames. The purposes of this paper are to interpret the Landsat cloud picture in terms of the atmospheric processes to demonstrate that these mesoscale processes resulted from differential heating of the cold land air over the ocean due in large part to the shape of the coast, and finally to show that the induced mesoscale circulation feeds back to affect the ocean. We also make some speculative conclusions concerning cyclogenesis.

2. Cloud Interpretation and Postulates

In addition to showing the primary features seen in the AVHRR photo in Fig. 10 of I[1], namely the main cloud streets oriented N-S in agreement with the surface winds (see Fig. 11 of I[1]) and cloud dimensions increasing downwind, consistent with the increasing depth of the mixed layer, Fig. 1 shows two other remarkable features which were not clearly discernable in the lower

[1]The figures in Chou and Atlas (1982) related to this study are reproduced in the Appendix for ease of access.

resolution TIROS-N imagery. These are: (1) the line of distinctly larger clouds, indicated as the curve AB and (2) clouds to the left of the latter curve are distinctly smaller than those to its right and are aligned in a general E-W direction as opposed to the N-S direction on the right. Our purpose is to show that these features are due to the establishment of a mesoscale circulation, and indeed, that the cloud line AB is a mesoscale front across which the low level winds shift sharply. We shall demonstrate how this mesoscale circulation is established and postulate some broader implications.

We suggest that the mesoscale circulation comes about in the following way. On this day (February 17, 1979) the wind coming off the shore is generally out of the north and is essentially constant in direction along the entire coast of Long Island and New Jersey. The wind speed is also virtually constant at 10 ms^{-1} over the region as seen at both the shore stations and the buoy about 75 km off the Long Island shore in Fig. 11 of I[1]. The wind speed at the buoy actually increases to a peak of about 12.5 ms^{-1} at about 0500 EST, but then subsides again (see Fig. 2). However its direction remains 350° ± 10° all day long. The temperature of the surface air on departing the Long Island and New Jersey coasts is also essentially the same; i.e., -16 to -14.4°C. The major difference in the air on either side of the postulated convergence line AB is thus due to the difference in the path length of overwater travel and the mean temperature of the underlying water surface (see Fig. 3 and the SST map of Fig. 12 in I[1]). To the west of the convergence line, the air along any latitude has had both a shorter path over water and a colder path averaged SST than the corresponding points to the east of the line.

The result is that the line AB represents a boundary between warmer air to the east with a relatively deep boundary layer and reduced surface pressures, and the colder air to the west with a shallow boundary layer and relatively high surface pressures. The differences in air temperature, boundary layer height, and surface pressure in an E-W direction across the line AB are such as to cause the low level winds to its west to accelerate to the east, in the manner of a sea breeze front. This is almost certainly the cause of the striking line of convergence and larger cloud elements which comprise the line AB.

To the east of the 'front', the clouds are clearly of a convective nature and continue to grow in horizontal dimension downstream, presumably in some proportion to the increasing depth of the boundary layer. Also in the eastern region, the cloud streets are oriented almost identically with the wind direction because of the very large heating rates there and the correspondingly large vertical momentum exchange, which precludes the existence of significant vertical shear.

To the west of the front, however, the clouds are not only smaller and oriented differently, but they are wavelike in character and show little evidence of changing wavelength in the N-S direction. It seems likely that the clouds in the western region are the result of Kelvin-Helmholtz waves whose orientation is perpendicular to the shear vector between the velocity of the mixed air in the shallow boundary layer (i.e., with a WNW component) and the strong NNW flow above. Such a shear vector would tend to have a N-S direction and thus give rise to the E-W cloud orientation. While, we have no ocean surface wind data to the west of the convergence line to confirm these explanations, and indeed very little to the east, we believe that the combination of the model results discussed below and the Landsat picture itself provide persuasive evidence in their support.

3. Model Results

In order to test the above hypotheses, we have used Stage and Businger's (1981 a, b) mixed layer model to compute the boundary layer height (Z_B), surface air temperature (T_o), and surface pressure (P_o) fields. The Stage and Businger model is a Lagrangian model. Assuming a steady state situation as qualified below, we are able to obtain the parameters Z_B, T_o, and P_o as function of the downwind distance; i.e., along a straight line running N-S parallel to the 'front' AB. Computations were made along 10 such parallel trajectories on both sides of the 'front', thus allowing the construction of maps of Z_B, T_o, and P_o. The initial temperature and humidity soundings at the New Jersey and the Long Island shores are assumed to be the same and are identical to those at JFK International Airport, New York at 1100 GMT 17 February 1979. The mean mixed layer wind speed is assumed to be 10 ms^{-1} with the wind blowing from the north and nearly perpendicular to

the Long Island shoreline. The divergence is taken to be 1.5×10^{-5} sec^{-1}. The sea surface temperature (SST) adopted is shown in Fig. 3 and is taken from the weekly mean SST (Fig. 12 of I[1]). The curve AB in Fig. 3 corresponds to the line of distinctly larger clouds in Fig. 1. It can be seen from Fig. 3 that the northerly air flow is generally across the SST isotherms in the region east of the curve AB, while the air flow is more nearly parallel to the SST isotherms to the west of AB. For the purpose of the present study we assume a steady state although it will become evident that the surface heating alters the initial meteorological fields, thus invalidating our assumption. Although the use of a time-dependent model would have been preferable, it seems clear that our basic findings would not have been altered in any major way.

Fig. 4 shows the map of the boundary layer height, surface air temperature and surface pressure generated from the Stage and Businger mixed layer model. Since it turns out that the Z_B and T_o contours are essentially concentric with the isobars, only the latter are shown in 1 mb steps. However, the corresponding values of Z_B and T_o are also labeled in Fig. 4. In estimating the surface pressure, it is assumed that the pressure-height relationship above the boundary layer is the same as that of the initial sounding. Therefore, the pressure at the boundary layer top (P_B) can be obtained from this relationship and the computed Z_B. The surface pressure (P_o) can then be estimated by integrating the hydrostatic equation from the boundary layer top (P_B) to the sea surface using the computed temperature and water vapor mixing ratio. The dashed curves in Fig. 4 indicate the synoptic scale pressure pattern, which is taken from the surface weather map of Fig. 11 of I[1] less 4 mb. The reason for adjusting the synoptic scale pressure field is that the surface pressure of the initial sounding at the shore is about 1036 mb (1100 GMT) instead of 1040 mb (1500 GMT) as indicated in the weather map. It can be seen from Fig. 4 that the mesoscale and the synoptic scale pressure patterns are in general agreement, except that the mesoscale field gives more detailed information around the curve AB. Also, the mesoscale N-S pressure gradient is in good agreement with that derived from the shore station at Islip, Long Island and the buoy about 75 km south (see Fig. 11 of I[1]). This amounts to 2.7×10^{-2} mb km^{-1} as compared with 2.4×10^{-2} mb km^{-1} in

our calculations. Note that the model generated surface air temperature at the buoy is also in good agreement with the observation, which is about -12° for the period 1200-1600 GMT.

It can be seen from Fig. 4 that the contours of P_0, Z_B, and T_0 virtually follow the configuration of the shoreline near the coasts of New Jersey and Long Island. Due to modification from the sea surface, however, the isopleths gradually change downstream to follow the SST isotherms, especially near the lower right corner of Fig. 4. This change occurs mainly on the western side of the 'front' because the isobaric pattern is generally parallel to the SST isotherms in the region east of the curve AB. Note that, at each isobar, the SST and the overwater paths are about the same for all the N-S trajectories to the east of the curve AB. This results in a simple situation there; i.e., the boundary layer is warming and growing (the surface pressure is dropping) downstream (southward) and the E-W pressure gradient is nearly negligible as compared to that on the western side.

On the other hand, the situation to the west of the curve AB is quite different. There, the air flow is more nearly parallel to the SST isotherms (which tend to parallel the coast) with the SST increasing eastward. More importantly, the overwater paths from shore also increase eastward. Therefore, the boundary layer height and the surface air temperature increase and the surface pressure decreases downstream and eastward to the curve AB.

It is strikingly clear from Fig. 4 that the differential heating over the ocean has given rise to the development of a strong mesoscale circulation and that the curve AB does indeed represent a front as originally postulated. We emphasize that the resulting pattern would remain essentially unchanged if we were to use a different boundary layer model. Only the gradients of T_0, Z_B, and P_0 would be altered.

With regard to the resulting effects on the winds in the boundary layer, these may be deduced reasonably by neglecting the Coriolis force on this scale. We see then that to the east of the front,

the winds would be accelerated down the pressure gradient and thus to the south. This is consistent with the orientation of the cloud streets. On the other hand, the strong west-east pressure gradient on the western side of the front would produce a westerly wind component there (discussed further below) thus giving rise to strong convergence at the front and the larger convective elements along the front which were responsible for our original suspicions.

It is now apparent that the induced changes in the wind speed and directions raise doubts about the original assumptions of steady state and unidirectional winds with which we started. Thus, it would have been desirable to use a 3-D time-dependent mesoscale model. However, we believe that our simple approach has in fact explained the dominant features. An interesting point is that the enhanced mesoscale pressure gradients on both sides of the front will not only accelerate the winds but also give rise to increased ocean-air heat fluxes. These, in turn, should further enhance the pressure gradients and winds in a positive feedback loop. Ultimately, of course, the boundary layer air temperature would approach that of the sea thus stopping further development. Some indirect evidence of such effects is seen in the wind speed trace at the buoy shown in Fig. 2. During the morning hours, after the temperature at the shore has reached its minimum value, the subsequent oceanic heating would be at a maximum. This would thus enhance the N-S pressure gradient and accelerate the winds. This is in fact what happened with a maximum in wind speed at 0500 EST after which the winds decreased once more.

By the way, the fact that the winds at the buoy did not alter direction during the day supports the assumption that Coriolis effects were negligible on these time and space scales. Of course, this could also reflect a balance between Coriolis deflection and a synoptic temporal variation.

In order to make a more quantitative estimate of the winds in the boundary layer to the west of the front, we have made an approximation to the solution. By neglecting the Coriolis force, the vertically averaged equation of motion may be written as (Lavoie, 1972)

$$dU/dt = -\rho^{-1}\ \partial p/\partial x - C_D\ U\,(U^2 + V^2)^{1/2}/(Z_B - h) \qquad (1)$$

$$dV/dt = -\rho^{-1}\ \partial p/\partial y - C_D\ V\,(U^2 + V^2)^{1/2}/(Z_B - h) \qquad (2)$$

where (x,y) is the traditional Cartesian coordinate system with the origin fixed at the Delaware coast, i.e., about (38.5°N, 75°W), t time, U and V the x and y components of the mean boundary layer velocity, respectively, ρ density, p pressure, C_D drag coefficient, and Z_B and h the heights of the mixed layer and the surface boundary layers, respectively. The value of h is generally much smaller than that of Z_B. In the Stage and Businger mixed layer model, h is assumed to be negligible as compared to Z_B, but the effects of the unstable surface boundary layer (superadiabatic temperature profile) on the mixed layer growth are included through the parameterizations of the fluxes of momentum, heat and moisture at the air-sea interface. Note that the values of Z_B and h are not needed for the following analysis. If we assume $dV/dt = 0$ and $dU/dt \simeq U\,\partial U/\partial x$, then (1) and (2) can be combined into

$$U\,\partial U/\partial x = -\rho^{-1}\ \partial p/\partial x + \rho^{-1}\ \partial p/\partial y\,(U/V) \qquad (3)$$

For the region around 38.5°N (y = 0) and between the Delaware coast and the curve AB, the x and y components of the mean surface pressure gradients are about 4.5×10^{-2} and 2.5×10^{-2} mb km^{-1}, respectively. If V = −10 m s^{-1} (uniform northerly wind), then (3) implies that the mesoscale pressure pattern can generate a westward wind component of about 9 ms^{-1} at x = 60 km with U = 0 near the shore (x = 0) and U = 18 ms^{-1} near the mesoscale front along AB (x = 120 km). The induced westerly wind component is therefore significant, again demonstrating the curve AB to be a convergence line similar to a sea breeze front.

4. The Cloud Streets

We now discuss the nature of the cloud streets on either side of the front in the light of the model results. The mean flow pattern of the boundary layer in the region west of the curve AB

may be deduced from the above analysis. Combining the gener l northerly flow with the westerly flow induced by the mesoscale pressure pattern, the flow patter tends to have a northerly wind initially (near the shore) and gradually turning into WNW flow when approaching the curve AB. Assuming a 300 m depth for the inversion la er and adopting the model calculated boundary layer height, the wind at the top of the inversion layer ($\hat{V}_T$) taken from the wind profiles at JFK International Airport, New York and Wallops Island, Virginia is about 22 ms^{-1} with NNW flow. This wind, $\hat{V}_T$, and that deduced in the boundary layer flow, $\hat{V}_B$, suggest a N-S vertical wind shear, $\hat{V}_Z$, across the inversion layer as shown in Fig. 5. This wind shear would trigger Kelvin-Helmholtz (K-H) instabilities in the inversion layer to produce billow clouds at the wave crests with the cloud axes perpendicular to the wind shear vector (Brown, 1980), i.e., essentially normal to the front as observed.

Kelvin-Helmholtz instability is a form of dynamic instability which occurs within a hydrostatically stable layer with strong vertical shear in the velocity profile. A necessary condition for the occurrence of K-H instability is that the local gradient Richardson number should be less than 0.25 (Miles and Howard, 1964). For the most unstable wave, the relationship between the wavelength (λ) and the thickness of the dynamically unstable shear layer (ΔZ) suggested by Miles and Howard (1964) and Woods (1969) is $\lambda = 7.5\ \Delta Z$ and that by Scorer (1969) is $\lambda = 4\pi\Delta Z$.

Figs. 6 and 7 show the roll wavelength (λ) and the aspect ratio (λ/Z_B) versus the distance downwind from the Long Island shore for the regions about 30 km east and west of the curve AB, respectively. The wavelength is visually estimated from the Landsat picture and the boundary layer height is taken from the model results. In the eastern region, the wavelength is about 3-10 km and the aspect ratio is about 3-7. These are in good agreement with the findings of Kuettner (1971) and LeMone (1973). Both the wavelength and the aspect ratio increase downstream with larger increases beyond 150 km of over water travel. This result, together with the fact that the cloud street orientation is essentially parallel to the mean wind in the boundary layer suggests that

the cloud streets to the east of the front are convective roll clouds in the boundary layer, which are caused by convective instability and the inflectional point instability as discussed by Kuettner (1971), Brown (1970, 1972), LeMone (1973), Lilly (1966), and others.

In the western region, on the other hand, the wavelength and the aspect ratio are virtually independent of fetch and are about 3 km and 3, respectively. Moreover, the wavelength appears to be independent of boundary layer height. This is also in agreement with the K-H instability theory that the most unstable wavelength is related to the thickness of the dynamically unstable shear layer (i.e., the inversion) and not to the boundary layer beneath it. The thickness of the inversion layer estimated from the aforementioned $\lambda - \Delta Z$ relations is in the range of 240 to 400 m if $\lambda = 3$ km, a not unreasonable result. Therefore, the cloud streets in the west are almost certainly "billow clouds" in the PBL capping inversion, which are due to Kelvin-Helmholtz instability. Assuming this to be correct, the orientation of the wave clouds and a knowledge of the winds above the inversion obviously provides information about the vector velocity of the winds in the boundary layer. In the present case, of course, we have deduced those winds from the model results, but they could have been estimated in the above described manner.

5. Impact on Ocean Waves

At least one other significant result may be deduced from the present findings. This relates to the feedback of the induced mesoscale circulation on the generation of ocean waves. Our associates at the Instrument Systems Division of this Center have been flying a sophisticated surface contour radar system to detect, measure, and display the structure and amplitude of ocean waves with a vertical resolution of 15 cm. The data from a swath some 500 m wide and 4 to 5 km in length is summarized in a two-dimensional Fourier analysis of the directional ocean wave spectra. Successive spectra for each segment along the flight path document the downwind evolution of the waves (Kenney, et al., 1979).

In order to study the development of fetch-limited waves, they have been flying on days of cold air outbreaks when the winds are strong and unidirectional in the hope of finding the simplest possible wave structure and determine the growth of wave amplitude and energy. Walsh[2] reports that even in these supposedly simple situations, in addition to the expected wave orientation perpendicular to the wind direction, there appears a mysterious secondary peak at another direction at distances of some 100 km off shore.

We suggest that the occurrence of such bimodal directional wave spectra on days when the synoptic scale surface flow is unidirectional may be attributable to the mesoscale windfield induced in the manner previously described. In the case shown, we have deduced the development of strong north westerly surface winds to the west of the mesoscale front in addition to the enhancement of the basic northerly flow to the east of that front. The waves generated by each of these winds will obviously travel across the frontal position so that in some swath of presently unknown dimensions centered along the front, one will find both wave directions in the spectra. In the case shown in Fig. 4, we expect the dominant waves to be oriented essentially E-W to the east of the front and to reach their peak amplitude along the front where the N-S fetch is bounded. On the south and west side of the front the latter waves will decay with distance from the front. Similarly, the NE-SW oriented waves generated by the induced north westerly winds to the west of the front will reach their peak amplitude at the front and decay with increasing distance to its east. The result is that the front represents the locus along which one will find both wave directions at their peak amplitude.

Unfortunately, Walsh[2] did not fly in a situation identical to the present one, nor does he have sufficient data to verify the above explanation. Thus, while this explanation seems entirely reasonable, it must be considered as a hypothesis to be tested in future flights. At the time of this writing Walsh[2] (private communication) believes that the second peak in his directional wave spectrum is due to swell and not to the process described here.

---

[2]Private communication from Dr. Edward Walsh of NASA/Goddard Space Flight Center, Instrument Systems Division.

6. Implications for Cyclogenesis

It takes no stretch of the imagination to suggest that the mechanism proposed here for the initiation of mesoscale circulations is somehow related to coastal cyclogenesis which is a climatological feature of the region near Cape Hatteras. Indeed, the now famous Presidents' Day Cyclone of February 18-19, 1979, which deposited record snowfalls along the middle Atlantic states, developed the day after the case we have discussed here. In an extensive study of that storm Bosart (1981) notes that

> "a region of enhanced lower tropospheric baroclinicity develops along the Carolina coastal strip in response to significant oceanic sensible and latent heat fluxes which warm, moisten and destabilize the boundary layer. Cyclogenesis is initiated along the coastal front as a result of lower tropospheric warm advection."

Recently, R. Atlas and R. Rosenberg[3] conducted numerical experiments to isolate the critical factors involved in the explosive development of the Presidents' Day Cyclone. The rapid intensification was correctly predicted with the GLAS[3] model operating in its standard mode. However, the model failed to predict cyclogenesis when the surface heat and moisture fluxes were cut off, thus demonstrating the crucial role of diabatic heating resulting from the oceanic fluxes. Of course, other large scale factors must also be favorable.

In our previous discussion we have emphasized the effects of the shape of the coast during off shore cold outflows. However, by 1200 GMT on February 18 the winds at all coastal stations in the Carolinas south of Cape Hatteras were directed on shore. The prior history of these air parcels showed that they left the New England coast with a northwesterly flow turning anticyclonically to approach the Carolinas from the east. Such a trajectory would have caused the boundary layer air to have been warmed and moistened throughout most of its oceanic passage. The air which would have been warmed the most is that which passed over the core of the Gulf Stream

---

[3] R. Atlas and R. Rosenberg, NASA Goddard Laboratory for Atmospheric Sciences (GLAS), private communication.

before reaching the shore. By analogy to our previous model results one can then visualize the temperature and height of the boundary layer rising, and the pressure falling with distance south of Cape Hatteras on February 18, thus producing the inverted trough in the pressure pattern (Bosart, 1981) which subsequently evolved into the coastal low. Incidentally, Sanders and Gyakum (1980) have previously suggested that the explosive development of coastal cyclones occurs preferentially near the strongest gradients of SST. This is not what we propose.

In short, we suggest that it is not only the warming and moistening of the low level air over the ocean which is responsible for the development of the coastal low, but also the pattern of that warming. This in turn must be related to the sea surface temperature pattern and the trajectories of the air relative to SST. While we are tempted to conclude that this is the reason for the climatological maximum of cyclogenesis in the vicinity of Cape Hatteras, we propose that the explanation be treated as a hypothesis for the time being. It would be most interesting to conduct numerical experiments with an ocean having a uniform temperature to determine whether coastal cyclogenesis also occurs under such circumstances, and other experiments to assess the role of the position and structure of the SST field.

7. Summary and Conclusions

In cases of cold air outbreaks, we have shown that the combination of the shape of the coast and the sea surface isotherms can have a profound effect in establishing a mesoscale atmospheric circulation as a result of differential heating due to both variations in overwater path length and the underlying SST. When the coastal effects dominate a mesoscale front forms downstream of the point marking the major bend in the orientation of the coastline. Moreover, the sea level isobars tend to parallel the shape of the coast, but pressure will always decrease with distance from shore as the boundary layer air is progressively warmed. Thus, when the coastline is concave towards the downwind direction a mesoscale low will form, and conversely when the coast is convex toward that direction. However, on the time and space scales treated here, the Coriolis effect will generally

not have time to work so that the induced winds will tend to accelerate across the isobars toward the low pressure.

The strength of the induced mesoscale circulation obviously depends upon the original thermal contrast between the land air and the SST. In any case, the mesoscale circulation and enhanced winds will in the first instance, feedback on the ocean by intensifying the wave growth and altering their directions. This is one of the possible reasons for the observation of bidirectional ocean wave spectra when the synoptic scale flow is unidirectional. The induced pattern of sea surface stress is also bound to have an additional effect on the coastal oceanic circulation, but this has not been discussed in the present paper.

It is worth noting that where the coastline and the isotherm pattern are more or less normal to the mean flow in the boundary layer, and the thermal contrast is sufficiently large, the cloud streets formed downstream will be convective in nature and oriented with the axes of roll vortices along the wind direction. The convective elements will also grow three dimensionally in the down-wind direction in rough proportion to the depth of the boundary layer.

On the other hand, where the mean wind in the boundary layer is nearly parallel to the coast-line and the SST isotherm pattern and the sea level isobars tend to parallel the coastline as noted earlier, one will establish a significant vertical wind shear across the inversion at the top of the boundary layer. The combination of the thermal stability and strong shear in this region is thus likely to give rise to Keivin-Helmholtz waves as observed in the Landsat picture of Fig. 1.

It is noteworthy that explosive cyclogenesis occurred on February 18-19, 1979, immediately following the day of the present study, giving rise to the famous Presidents' Day cyclone. Bosart (1981) and R. Atlas and Rosenberg[3] (private communication) agree that the oceanic fluxes of heat and moisture were critical to the development of this storm. However, we hypothesize that it is the differential heating resulting from the passage of air over the sea surface temperature pattern

which is probably the crucial factor. This may explain the climatological peak frequency of cyclogenesis in the vicinity of Cape Hatteras which is downwind of the core of the Gulf Stream when the surface winds are from the east or northeast.

Finally we note that almost none of the above interpretations would have been possible without the high resolution Landsat pictures. We believe that an understanding of many such physical processes will emerge from the detailed study of such high resolution imagery and recommend that meteorologists and oceanographers exploit them fully.

Acknowledgements

We are most grateful to Mr. William Byerly of Systems and Applied Sciences Corporation for his enthusiastic effort on programming and data analysis. We were also inspired by enlightening discussions with many of our colleagues in GLAS, most particularly Drs. Robert Atlas, Eugenia Kalnay, Milton Halem, Joanne Simpson, D. B. Rao, Michael C. McCumber, and Paul Schopf. We also appreciate the general assistance of Messrs. Earl Kreins and William C. Skillman and the fine typing and editorial work of Mrs. Sharon Anderson, of NASA/Goddard Laboratory for Atmospheric Sciences.

REFERENCES

Bosart, L. F., 1981: The Presidents' Day snowstorm of 18-19 February 1979: A subsynoptic scale event. *Mon. Wea. Rev.*, 109, 1542-1566.

Brown, R. A., 1970: A secondary flow model for the planetary boundary layer. *J. Atmos. Sci.*, 27, 742-757.

_____, 1972: On the inflection point instability of a stratified Ekman boundary layer. *J. Atmos. Sci.*, 29, 850-859.

_____, 1980: Longitudinal instabilities and secondary flows in the planetary boundary layer: A Review. *Rev. Geophys. Spa. Phys.*, 18, 683-697.

Chou, S. H., and D. Atlas, 1982: Estimating ocean-air heat fluxes during cold air outbreaks by satellite. Submitted to the *Mon. Wea. Rev.*

Kenney, J. E., E. A. Uliana, and E. J. Walsh, 1979: The Surface contour radar, a unique remote sensing instrument. *IEEE Trans., Microwave Theory and Techniques,* MTT-27, 1080-1092.

Kuettner, J., 1971: Cloud bands in the earth's atmosphere: Observations and theory. *Tellus,* 23, 404-425.

Lavoie, R. L., 1972: A mesoscale numerical model of lake-effect storms. *J. Atmos. Sci.*, 29, 1025-1040.

LeMone, M. A., 1973: The structure and dynamics of horizontal roll vortices in the planetary boundary layer. *J. Atmos. Sci.*, 30, 1077-1091

Lilly, D. K., 1966: On the stability of Ekman boundary flow. *J. Atmos. Sci.*, 23, 481-494.

Miles, J. W., and L. N. Howard, 1964: Note on a heterogeneous shear flow. *J. Fluid Mech.*, 20, 331-336.

Sanders, F., and J. R. Gyakum, 1980: Synoptic dynamic climatology of the bomb. *Mon. Wea. Rev.*, 108, 1589-1606.

Scorer, R. S., 1969: Billow mechanics. *Radio Science*, 4, 1299-1308.

Stage, S. A., and J. A. Businger, 1981a: A model for entrainment into a cloud-topped marine boundary layer – Part I: Model description and application to a cold air outbreak episode. *J. Atmos. Sci.*, 38, 2213-2229.

_____, and _____, 1981b: A model for entrainment into a cloud-topped marine boundary layer – Part II: Discussion of model behavior and comparison with other models. *J. Atmos. Sci.*, 38, 2230-2242.

Wood, J. D., 1969: On Richardson's number as a criterion for laminar-turbulence-laminar transition in the ocean and atmosphere. *Radio Science*, 4, 1289-1298.

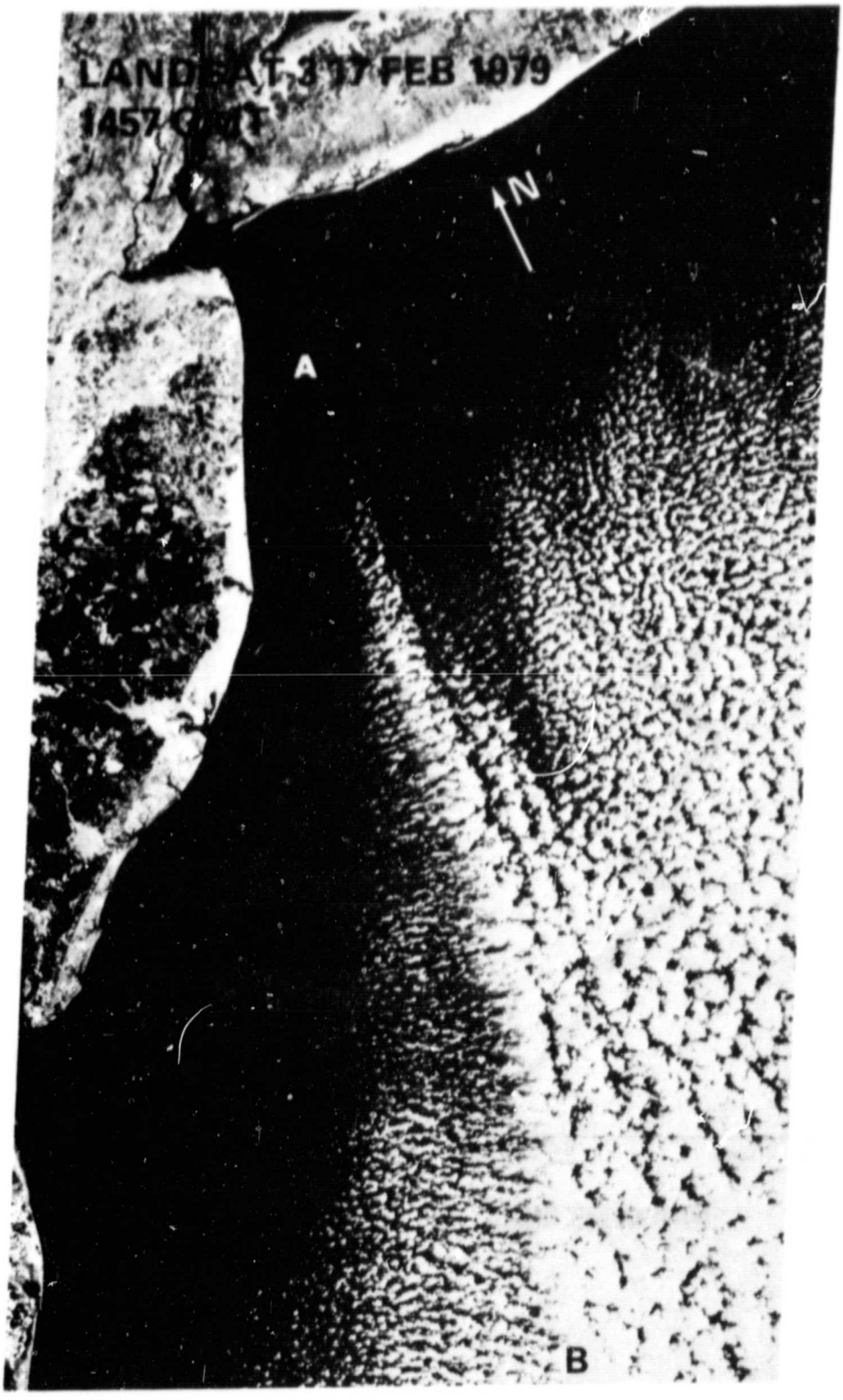

Figure 1. Cold air outbreaks on 17 February 1979 as seen by Landsat-3 visible channel at 1457 GMT. See text for the explanation on the curve AB.

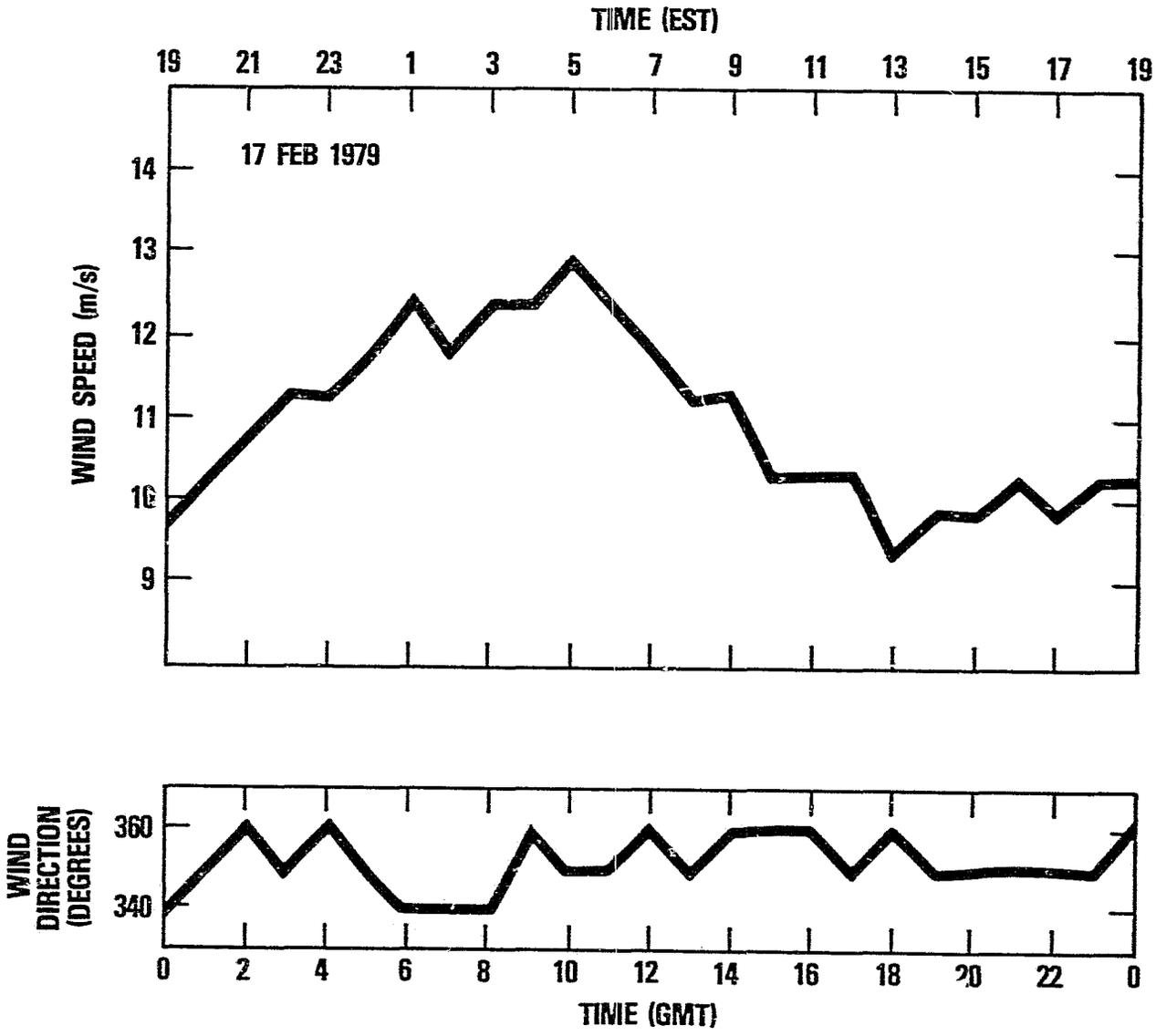

Figure 2. Diurnal variations in the wind speed and direction for 17 February 1979 at the buoy about 75 km south of Long Island shore, New York. See Fig. 3 for the location of the buoy.

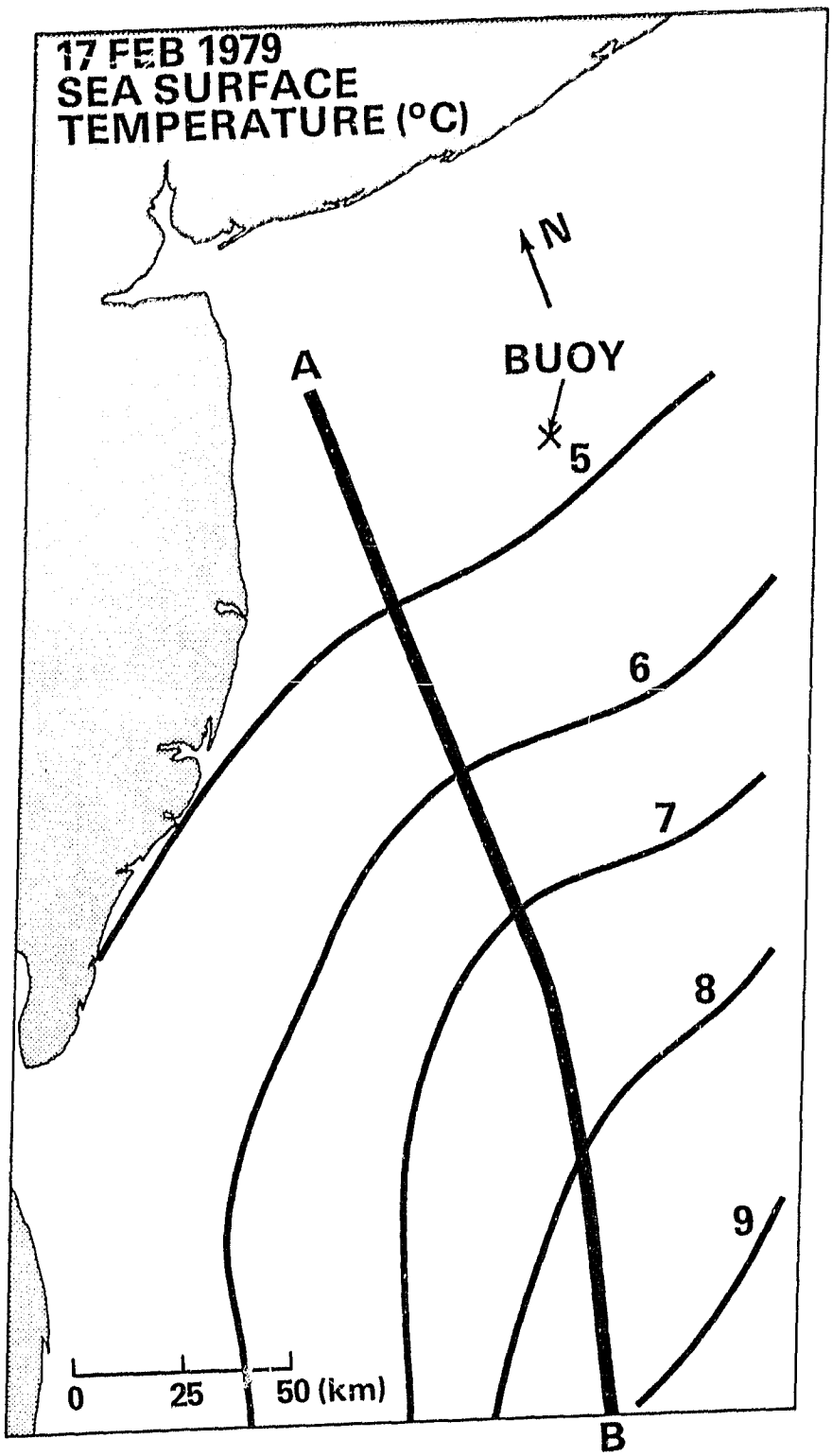

Figure 3. Weekly mean sea surface temperature for the period 14-21 February 1979. "X" indicates the position of the buoy.

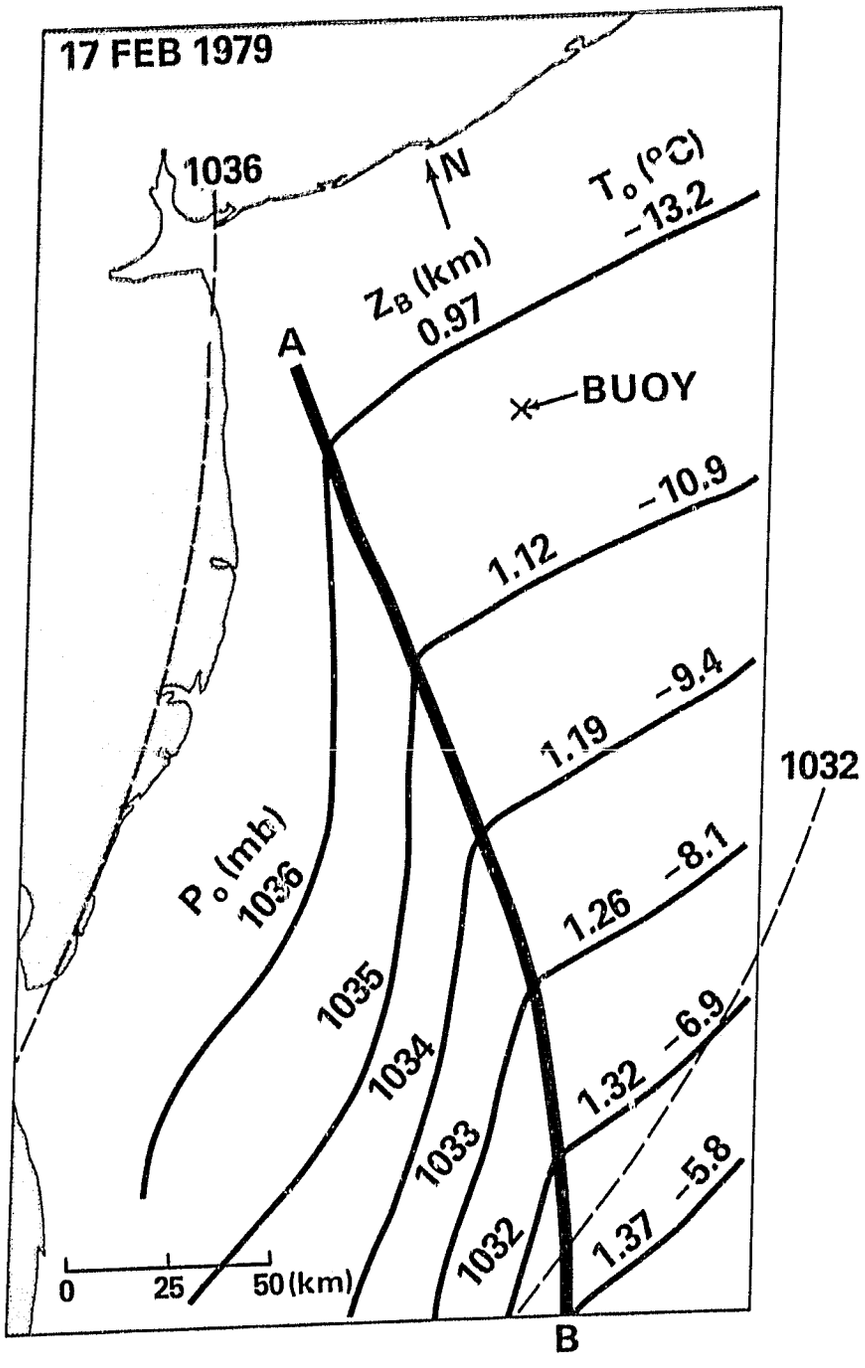

Figure 4. The boundary layer height (Z_B), the surface air temperature (T_o) and the surface pressure (P_o) generated from Stage and Businger's (1981a, b) mixed layer model (solid curves). The dashed curves correspond to the synoptic scale pressure pattern of Fig. 11 in Chou and Atlas (1982) less 4 mb. "X" indicates the position of the buoy.

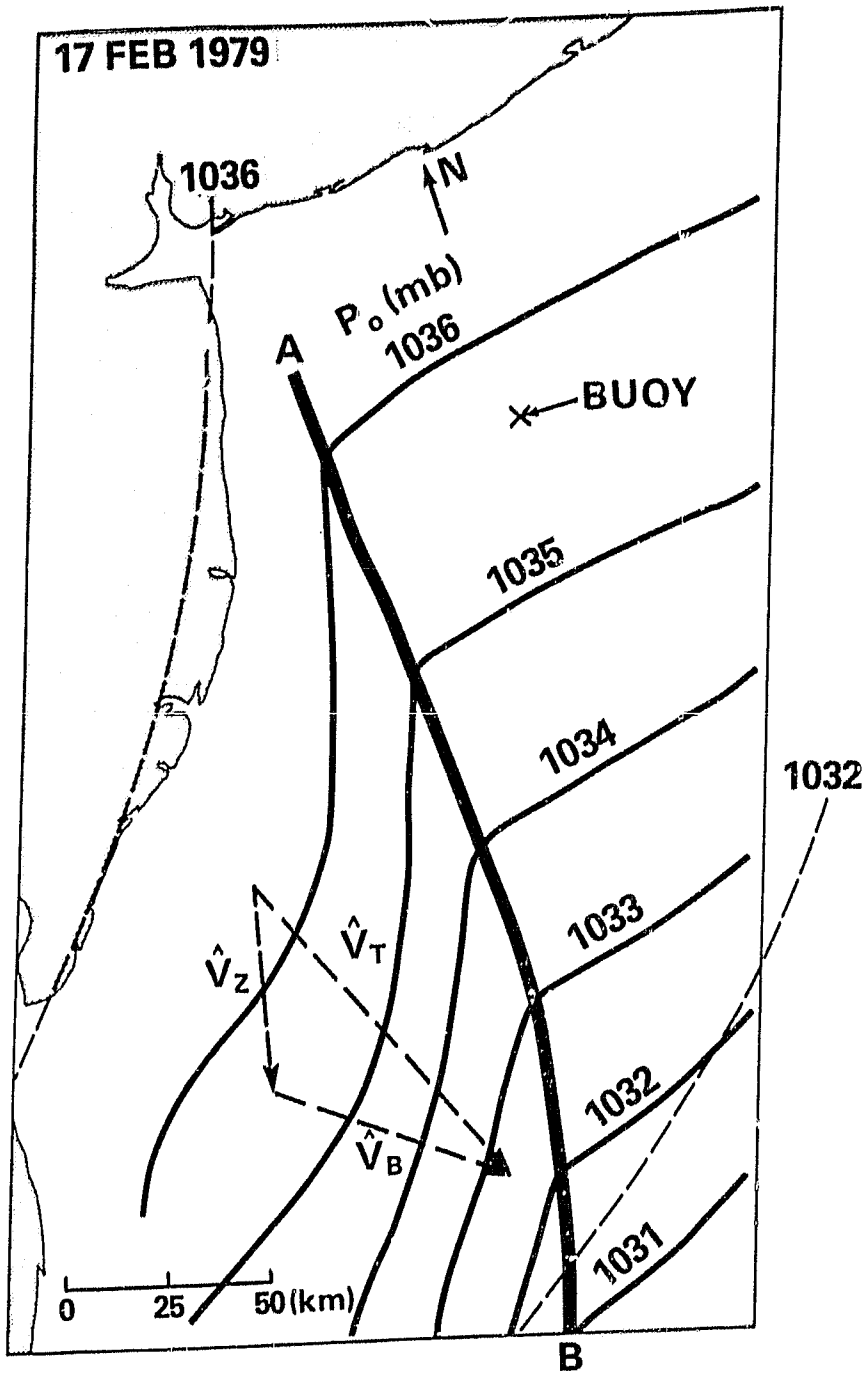

Figure 5. Wind shear vector across the inversion layer for the region west of the mesoscale front. $\hat{V}_T$ is the wind at the top of the inversion layer, $\hat{V}_B$ is the wind in the mixed layer, and $\hat{V}_Z$ is the wind shear across the inversion layer. The cloud streets are perpendicular to the wind shear vector $\hat{V}_Z$.

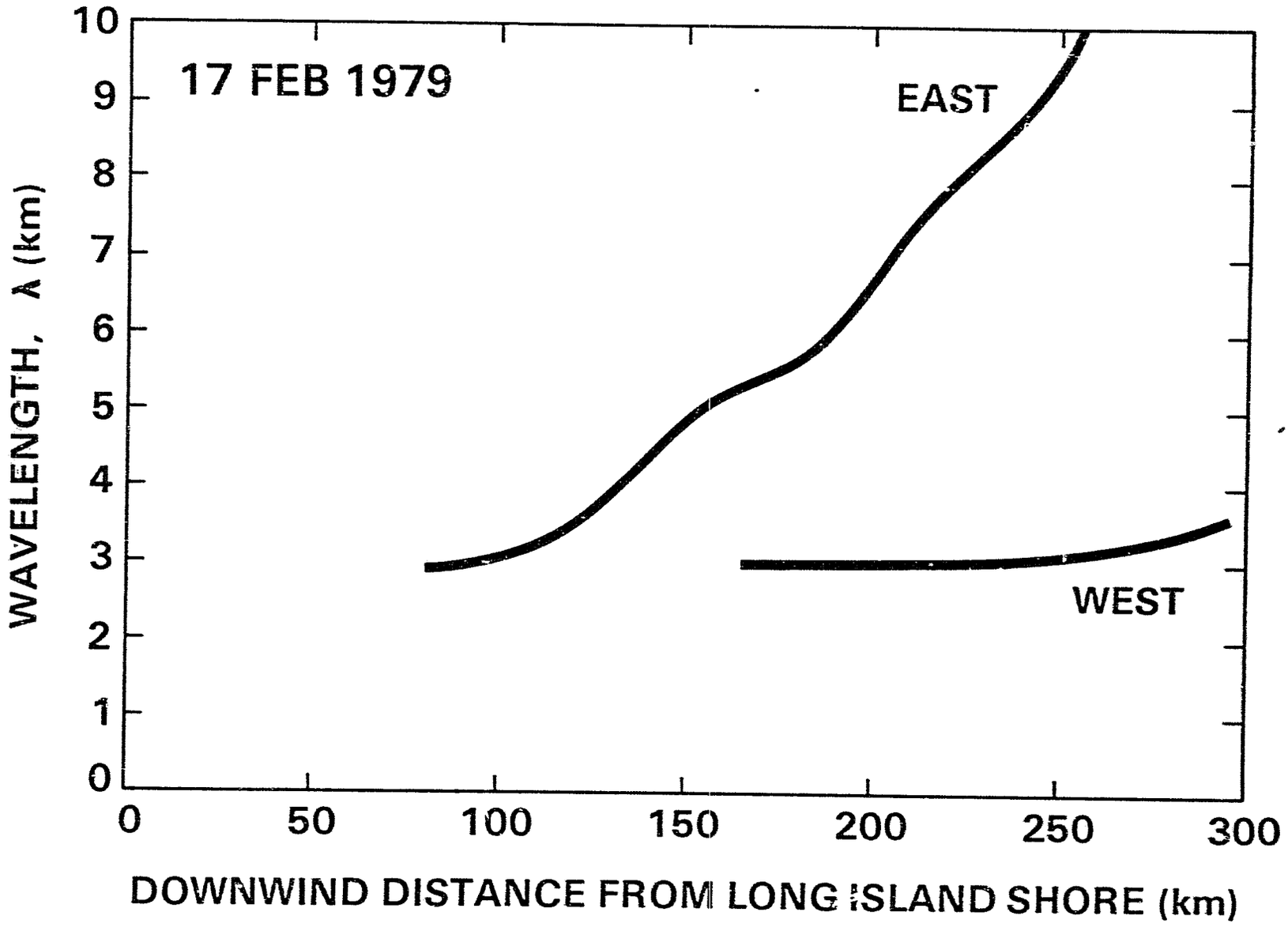

Figure 6. Roll wavelength versus the distance downwind from the Long Island shore for the regions about 30 km east and west of the mesoscale front. Wavelength is estimated from the Landsat picture.

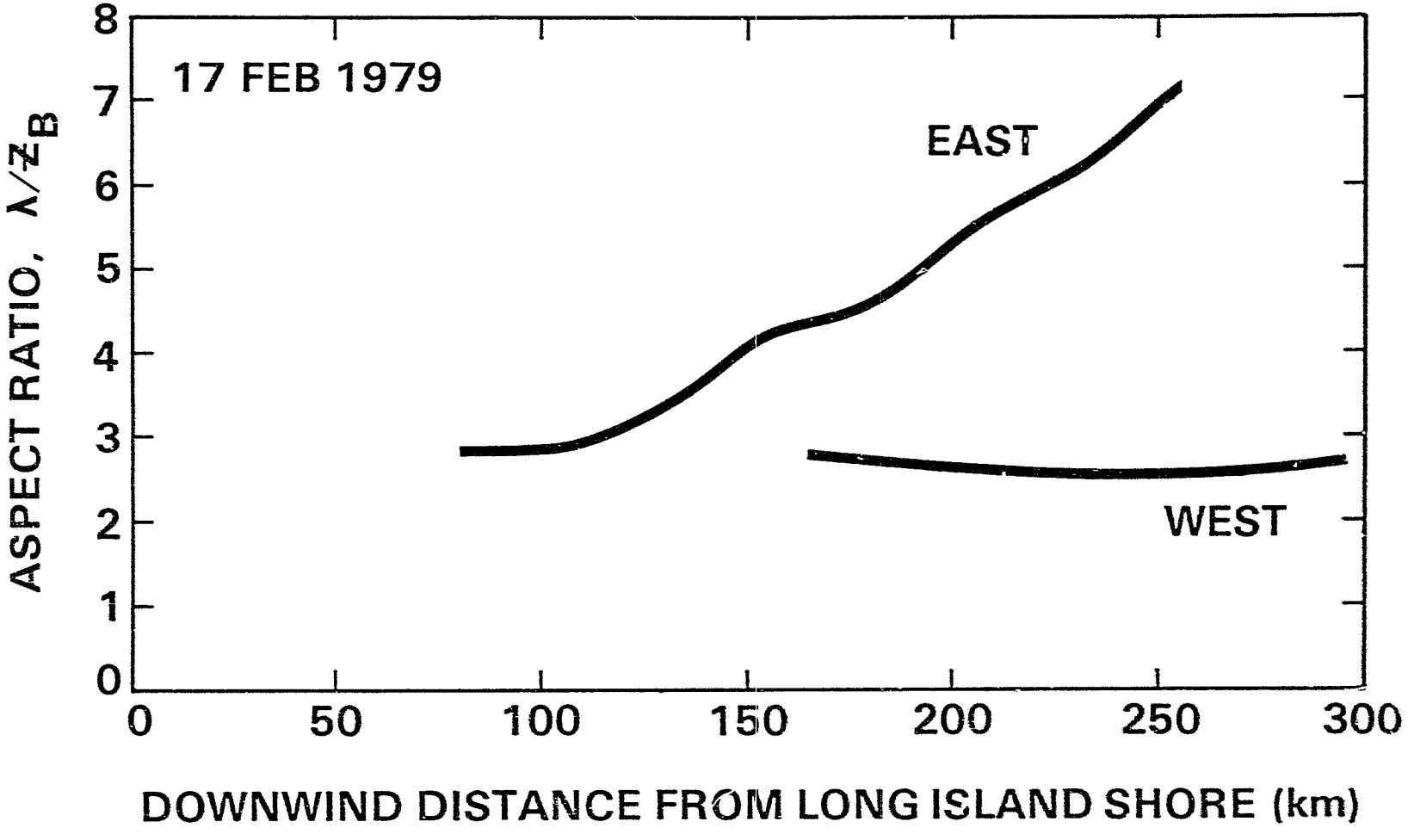

Figure 7. Aspect ratio (λ / Z_B) versus the distance downwind from the Long Island shore for the regions about 30 km east and west of the mesoscale front. Wavelength (λ) is estimated from the Landsat picture and the boundary layer height (Z_B) is taken from the results of Stage and Businger's (1981 a, b) mixed layer model.

APPENDIX

Related Figures of Chou and Atlas (1982)

The Figures in Chou and Atlas (1982) related to this paper are reproduced here for ease of access. The figure numbers are identical to those in Chou and Atlas (1982).

ORIGINAL PAGE
BLACK AND WHITE PHOTOGRAPH

Figure 10. Cold air outbreak on 17 February 1979 as seen by Tiros-N AVHRR IR channel at 1941 GMT. Abscissa and ordinate are marked in longitude and latitude. Cloud streets south of Long Island, New York are aligned in the N-S direction. (Reproduced from Chou and Atlas, 1982 without color.)

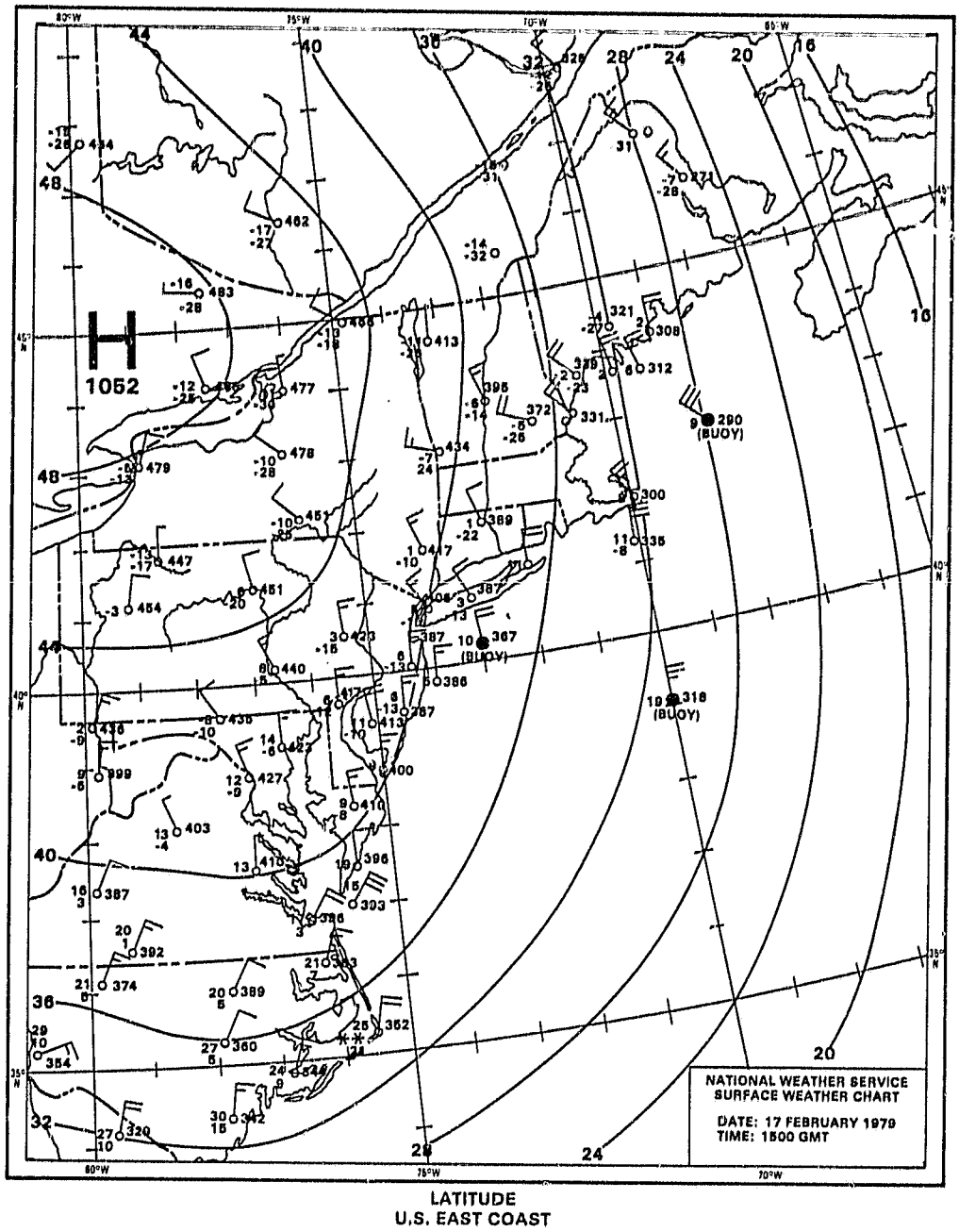

Figure 11. Surface weather map of 17 February 1979 at 1500 GMT. (Reproduced from Chou and Atlas, 1982.)

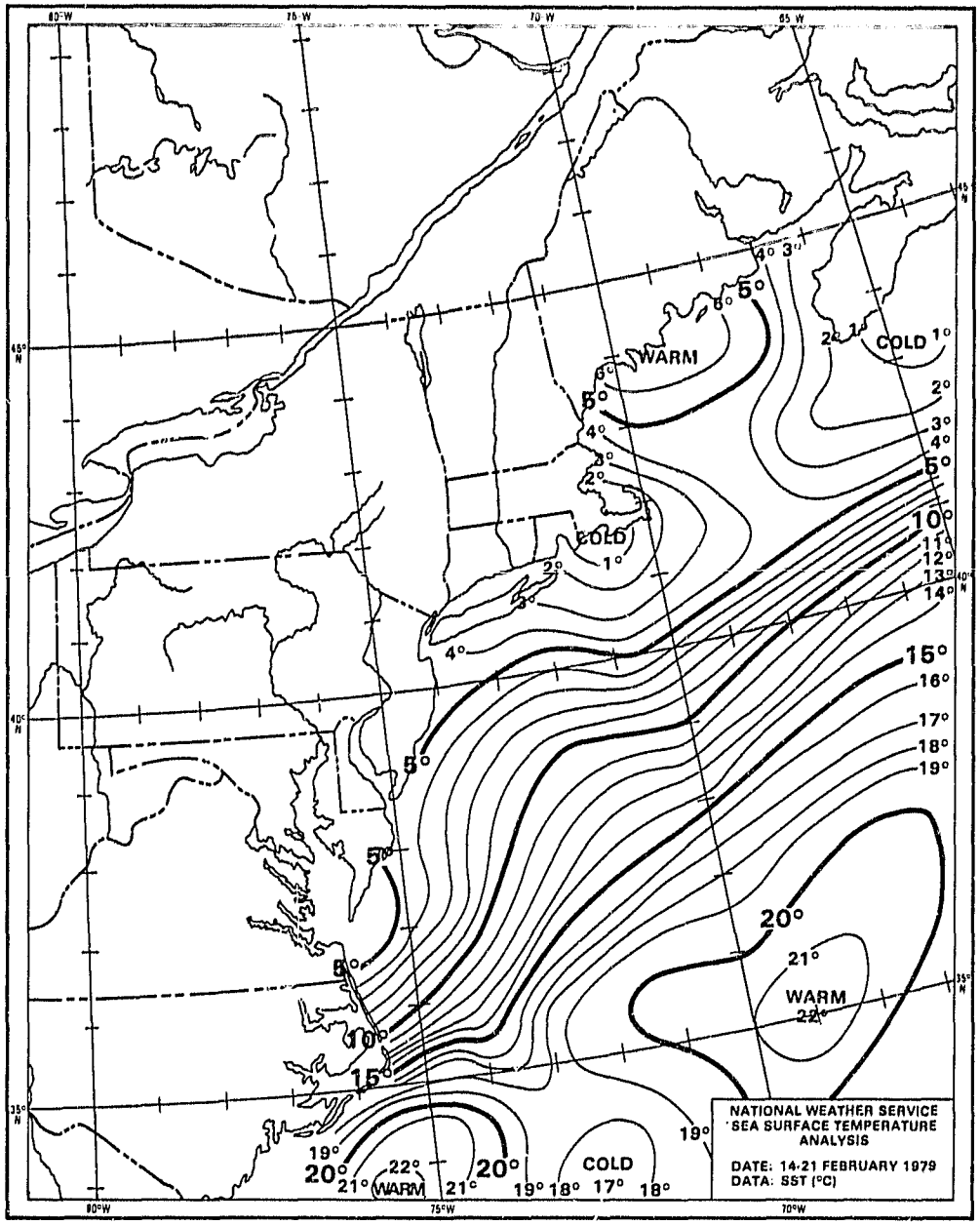

Figure 12. Weekly mean sea surface temperature for the period 14-21 February 1979. (Reproduced from Chou and Atlas, 1982.)

FIGURE CAPTIONS

Figure 1. Cold air outbreaks on 17 February 1979 as seen by Landsat-3 visible channel at 1457 GMT. See text for the explanation on the curve AB.

Figure 2. Diurnal variations in the wind speed and direction for 17 February 1979 at the buoy about 75 km south of Long Island shore, New York. See Fig. 3 for the location of the buoy.

Figure 3. Weekly mean sea surface temperature for the period 14-21 February 1979. "X" indicates the position of the buoy.

Figure 4. The boundary layer height (Z_B), the surface air temperature (T_o) and the surface pressure (P_o) generated from Stage and Businger's (1981a, b) mixed layer model (solid curves). The dashed curves correspond to the synoptic scale pressure pattern of Fig. 11 in Chou and Atlas (1982) less 4 mb. "X" indicates the position of the buoy.

Figure 5. Wind shear vector across the inversion layer for the region west of the mesoscale front. $\hat{V}_T$ is the wind at the top of the inversion layer, $\hat{V}_B$ is the wind in the mixed layer, and $\hat{V}_Z$ is the wind shear across the inversion layer. The cloud streets are perpendicular to the wind shear vector $\hat{V}_Z$.

Figure 6. Roll wavelength versus the distance downwind from the Long Island shore for the regions about 30 km east and west of the mesoscale front. Wavelength is estimated from the Landsat picture.

Figure 7. Aspect ratio (λ/Z_B) versus the distance downwind from the Long Island shore for the regions about 30 km east and west of the mesoscale front. Wavelength (λ) is estimated from the Landsat picture and the boundary layer height (Z_B) is taken from the results of Stage and Businger's (1981 a,b) mixed layer model.

Figure 10. Cold air outbreak on 17 February 1979 as seen by Tiros-N AVHRR IR channel at 1941 GMT. Abscissa and ordinate are marked in longitude and latitude. Cloud streets south of Long Island, New York are aligned in the N-S direction. (Reproduced from Chou and Atlas, 1982 without color.)

Figure 11. Surface weather map of 17 February 1979 at 1500 GMT. (Reproduced from Chou and Atlas, 1982.)

Figure 12. Weekly mean sea surface temperature for the period 14-21 February 1979. (Reproduced from Chou and Atlas, 1982.)